CFD STUDY OF GAS FLOW THROUGH STRUCTURED SEPARATION COLUMNS PACKINGS MELLAPAK 250.X AND MELLAPAK 250.Y

M. Isoz [1,2]

[1] **Department of Mathematics, Faculty of Chemical Engineering, University of Chemistry and Technology, Studentska 5, 166 28 Prague, Czech Republic**
[2] **Institute of Thermomechanics, Czech Academy of Sciences, Dolejskova 5, 182 00 Prague, Czech Republic**

Abstract

In order to increase the size of the gas-liquid interface area and consequently the intensity of the mass transfer, the separation columns are usually filled with a geometrically complex packing. The packing highly increases intricacy of the flow in the column and also makes almost all types of hydrodynamic measurements impossible. Hence a reliable model of the flow in the complex geometry of the separation column packing is sought by the industry. We provide a CFD model for the gas flow through two types of commercial structured packings, Mellapak 250.X and Mellapak 250.Y. We validate the model on experimental data and use it to study the gas mixing capabilities of the packings.

Keywords: CFD, OpenFOAM, structured packing, distillation, absorption.

1 Introduction

The U.S. Department of Energy estimates that the distillation columns are responsible for approximately 40% of the total energy consumption of the U.S.'s chemical industry [7]. Also, based on a recent report on the energy consumption in the European Union[4], the chemical industry participated on the total 2014 energy consumption of the European Union by 5%. As the structure of the chemical industry in the European Union and United States is, in overall, similar, it is possible to estimate, that in 2014 the distillation columns caused approximately 2% of the total energy consumption of the whole European Union. In absolute values, this roughly corresponds to 32 million tonnes of oil equivalent (or $372 \cdot 10^6$ MWh) per year[4].

Despite the energy-intensity of the distillation, the design of the separation columns is still mostly empirical [19]. On the other hand, even a slight advancement in design or operation would result in substantial cost savings. Hence, improvements in the distillation column design are currently viewed as the biggest opportunity to increase the European chemical industry efficiency and sustainability[21].

One of the reasons of the current state of the distillation column design is the shear complexity of the involved technology. For example, due to the intricacies of the separations columns internals, it is almost impossible to directly measure the hydrodynamic properties of these devices. Furthermore, the modeling of the foretold phenomenon has long been constrained by the lack of both the necessary computing power and suitable models.

On the other hand, with the recent increase in available computational resources, the methods of computational fluid dynamics (CFD) may be, in particular for the case of a single phase flow, applied directly to resolve the flow in the whole column at once. This development inspired a number of recent studies in this area. The overall review of the CFD methods available for the design of packed absorption columns was recently given by Haroun and Raynal [9]. Besides, Owens et al. [15] developed an approach to modeling the gas flow through widely used structured packing, Mellapak 250.Y. They suggested the use of X-ray computed tomography (CT) for the model geometry generation. Therefore, their model construction requires the availability of an actual packing. However, the rest of the modeling proces is automatic and the results can be obtained within hours. Aside from the above, Amini et al. [1] used a CFD model to complete an experimental performance evaluation of a new type of structured packing and to speed up the packing design process. Nevertheless, the CFD modeling is not limited only to the structured packings and for example Parizi and Rahimi [16] used CFD to study the hydrodynamics of a sieve tray distillation column. Interestingly, not many results are available for the random packings

and the few existing results are oriented towards packed bed reactors and either a spherical or cylindrical packing (e.g. Baker [3], Bai et al. [2]).

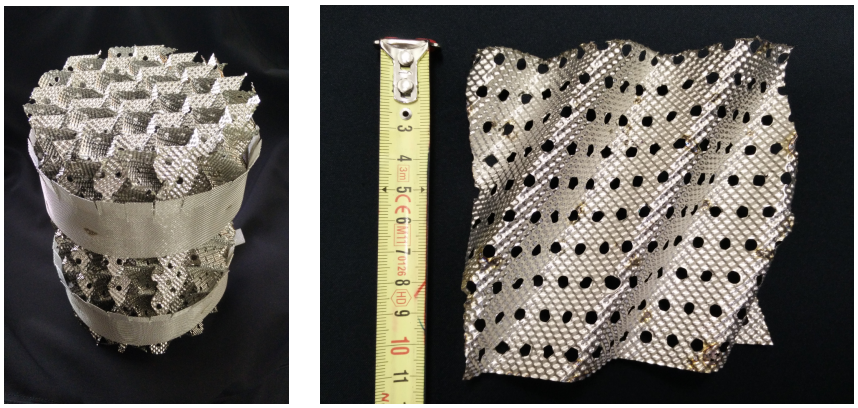

Figure 1: Example of a separation column packing – Mellapak 250.Y. An overall view of the packing is depicted on the left. On the right, there is shown a detail of one element of a dismantled packing. Structured packing usually consists of corrugated, perforated and textured steel plates. Standard mode of operation is counter-current: liquid phase flows down and gas phase up.

Furthermore, besides the studies performed on the whole separation column geometry, there exists a notable amount of results calculated on so called representative elementary units (REUs). Structured packings are highly regular structures (see Fig. 1). Raynal and Royon-Lebeaud [17] leveraged the regularity of the structured packings and proposed an approach based on a segmentation of the problems into three ranges of spatial scales: (i) the micro-scale REU which is to be resolved directly via a full CFD model, (ii) the meso-scale corresponding to one element of the packing material, and (iii) the macro-scale, which coincides with the full column. The idea behind the approach of Raynal and Royon-Lebeaud is to solve exactly only a small portion of the complex geometry involved, REU, and to use the obtained information to construct an approximate model of the larger spatial scales. Such approach is computationally less demanding process than CFD simulation of the whole macro-scale column. Hence, it enables detailed studies of a multiphase flow [6, 10] coupled with heat and mass transfer [20].

In addition to the results on applications of the CFD models to the specific industrial problems there exist several studies of effects of different approaches to the modeling itself. As an example, we would like to mention the work by Khosravi-Nikou and Eshani [12], who evaluated effects of the turbulence model selection on the simulation results.

In the present work, we provide a CFD model for the gas flow in two types of widely used commercial packings, Mellapak 250.X and Mellapak 250.Y. First, we validate the proposed model against experimental data via a comparison of measured and calculated packing dry pressure loss. Then we use the validated model to inspect the Mellapak 250 gas mixing capabilities.

Our overall approach used for the simulation construction was similar to the work of Owens et al. [15] with the turbulence modeling based on the results of Khosravi-Nikou and Eshani [12]. The simulations were carried out in the OpenFOAM software. The OpenFOAM is an open-source finite volume method (FVM) based solver. It focuses primarily on issues of the computational continuum mechanics. As a tool for the packing geometry creation, we applied the Blender, an open-source 3D creation suite. Combining Blender and OpenFOAM, we were able to generate the structured packing geometry and the corresponding mesh automatically. It makes the model completely independent on the availability of the real packing and thus suitable for packing design.

2 Computational domain and meshing

The Mellapak 250 packing is a geometrically highly complex structure, as it may be seen in Fig. 1. Thus, a robust tool has to be used for a suitable FVM mesh creation. As a suitable tool, we selected snappyHexMesh utility available in the OpenFOAM core installation. SnappyHexMesh

requires a representation of the geometry, which we created within the Blender software suite. One example of a whole geometry of one packing element with a diameter $D_{\mathrm{pk}} = 0.14\,\mathrm{m}$ and height $H_{\mathrm{pk}} = 0.21\,\mathrm{m}$ is depicted on the left side of Fig. 2.

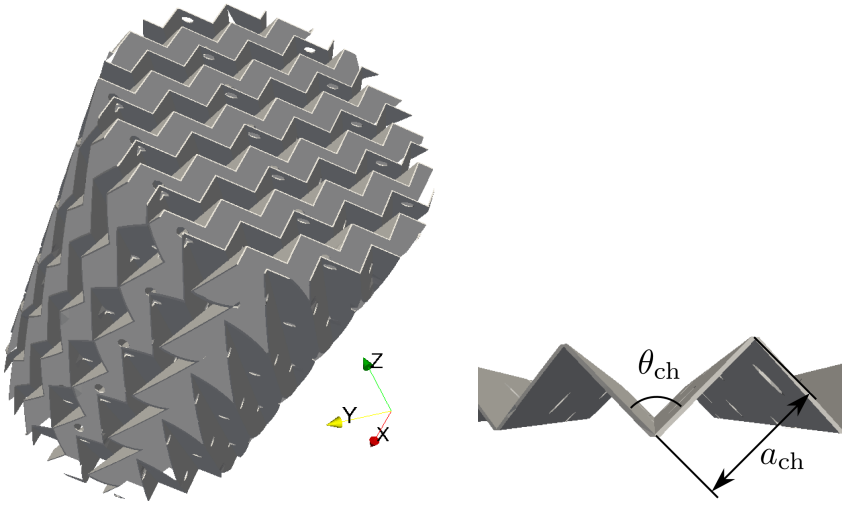

Figure 2: Geometry of one packing element of the Mellapak 250.X packing is depicted on the left side. On the right side, a detail of one packing channel is shown.

The process of the geometry creation leverages the regularity of the Mellapak packing structure. More specifically, the packing is formed by a series of channels with a triangular cross-section as it is shown on the right side of Fig. 2. Thus the geometry of the Mellapak packing can be described using only several different parameters, namely the dimensions of one channel, the channel side length, a_{ch}, and the angle between the channel sides, θ_{ch}, the number of channels appertaining to one corrugated metal sheet, N_{ch}, the channel inclination to the horizontal, α_{ch}, the number of metal sheets to be created, N_{sh} and the overall size of the packing described by D_{pk} and H_{pk}. Furthermore, it is possible to describe the packing perforation by the diameter of one hole, D_{pr}, and the distance between the centers of two adjacent holes, a_{pr}. Finally, the whole packing bed might be defined by the number of the packing elements, N_{pk}, and the respective rotation of the two adjacent packing elements, φ_{pk}. The last parameter required for the geometry creation is the thickness of the used metal sheets. This parameter was fixed at $w_{\mathrm{sh}} = 0.5\,\mathrm{mm}$ as finner sheets caused instabilities during the meshing process.

The geometry creation is specified in Alg. 1. For the clarity of the notation, we use a combination of a global Cartesian coordinate system (O, x, y, z) with a local coordinate systems $(\tilde{O}_i, \tilde{x}_i, \tilde{y}_i, \tilde{z}_i)$. The center of the local coordinate system, $\tilde{O}_i$, is fixed at the centroid of the object i and the local axis $(\tilde{x}_i, \tilde{y}_i, \tilde{z}_i)$ are parallel with the global ones, (x, y, z).

Using the Alg. 1, it is possible to create a usable geometry for the Mellapak type packing within minutes. As also the rest of the modeling process can be fully automated, it is possible to study the dependence of the flow behavior on the geometry parameters. Furthermore, additional features, such as the collars (or wall wipers) visible on the left side of Fig. 1 can be easily added to the geometry. Examples of geometry of the packed beds consisting of Mellapak 250 packing elements are depicted in Fig. 3.

The outputs of the Alg. 1 were imported in the OpenFOAM meshing tool, the snappyHexMesh. The snappyHexMesh utility generates three-dimensional meshes containing hexahedra (hex) and split-hexahedra (split-hex) automatically from triangulated surface geometries . As a core part of the OpenFOAM software, the snappyHexMesh is specialized on FVM calculations.

The mesh approximately conforms to the surface by iteratively refining starting mesh and morphing the resulting split-hex mesh to the surface . The mesh quality is repetitively controlled and adjusted during the meshing process, which enables the snappyHexMesh to provide high quality meshes even for complex geometries such as the studied Mellapak type packing. Furthermore, the utility is suitable for paralelization, scales well even on hundreds of cores and thus is applicable

Algorithm 1 Mellapak type geometry creation

Require: Packing geometry parameters: $a_{\mathrm{ch}}, \theta_{\mathrm{ch}}, N_{\mathrm{ch}}, \alpha_{\mathrm{ch}}, N_{\mathrm{sh}}, D_{\mathrm{pk}}, H_{\mathrm{pk}}, D_{\mathrm{pr}}, a_{\mathrm{pr}}, N_{\mathrm{pk}}, \varphi_{\mathrm{pk}}, w_{\mathrm{sh}}$

Create the first channel side, s_1, of dimensions $a_{\mathrm{ch}} \times 2D_{\mathrm{pk}}/\sin\alpha_{ch} \times w_{\mathrm{sh}}$ at position $\boldsymbol{x}_{s_1} = ((a_{\mathrm{ch}} - w_{\mathrm{sh}})\cos\theta_{\mathrm{ch}}, 0, 0)^{\mathrm{T}}$;
Rotate s_1 by $\theta_{\mathrm{ch}}/2$ along the $\tilde{y}_{s_1}$ axis;
for $i = 2$ **to** $2N_{\mathrm{ch}}$ **do**
  Duplicate the previous channel side, $s_i \leftarrow s_{i-1}$;
  Update the location of s_i, $\boldsymbol{x}_{s_i} = (i(a_{\mathrm{ch}} - w_{\mathrm{sh}})\cos\theta_{\mathrm{ch}}, 0, 0)^{\mathrm{T}}$;
  Rotate s_i by $(i \mod 2)\theta_{\mathrm{ch}}$ along the $\tilde{y}_{s_i}$ axis;
end for
Join all the channel sides to one corrugated sheet, $S_1 := \bigcup_{i=1}^{2N_{\mathrm{ch}}} s_i$;
Update the position of the global coordinate system, $(O, x, y, z) := (\tilde{O}_{S_1}, \tilde{x}_{S_1}, \tilde{y}_{S_1}, \tilde{z}_{S_1})$;
Rotate S_1 by $-\alpha_{\mathrm{ch}}$ along the $\tilde{z}_{S_1}$ axis;
for $i = 2$ **to** N_{sh} **do**
  Duplicate the previous sheet, $S_i \leftarrow S_{i-1}$;
  Update the location of S_i, $\boldsymbol{x}_{S_i} = (0, 0, (i - \mathrm{floor}\,(N_{\mathrm{sh}}/2))a_{\mathrm{ch}}\sin\theta_{\mathrm{ch}})^{\mathrm{T}}$;
  Rotate S_i by $(-1)^i\alpha_{\mathrm{ch}}$ along the $\tilde{z}_{S_i}$ axis;
end for
Join all the sheets to one packing element, $P_1 := \bigcup_{i=1}^{N_{\mathrm{sh}}} S_i$;
Update the position of the global coordinate system, $(O, x, y, z) := (\tilde{O}_{P_1}, \tilde{x}_{P_1}, \tilde{y}_{P_1}, \tilde{z}_{P_1})$;
Cut out the cylindrical shape of the packing, $P_1 := \{(x, y, z) \in P_1 : y^2 + z^2 \leq D_{\mathrm{pk}}^2/4 \wedge |x| \leq H_{\mathrm{pk}}/2\}$
Create the perforation, $P_1 := P_1 \backslash \{(x, y, z) \in P_1 : (x - ia_{\mathrm{pr}})^2 + (y - ja_{\mathrm{pr}})^2 \leq D_{\mathrm{pr}}^2/4\}_{i,j\in\mathbb{Z}}$;
for $i = 2$ **to** N_{pk} **do**
  Duplicate the previous packing element, $P_i \leftarrow P_{i-1}$;
  Update the location of P_i, $\boldsymbol{x}_{P_i} = ((1/2 + i - 2)H_{\mathrm{pk}}, 0, 0)^{\mathrm{T}}$;
  Rotate P_i by $(i \mod 2)\varphi_{\mathrm{pk}}$ along the $\tilde{x}_{P_i}$ axis;
end for
Join all the packing elements to a packed bed, $B := \bigcup_{i=1}^{N_{\mathrm{pk}}} P_i$;
Update the position of the global coordinate system, $(O, x, y, z) := (\tilde{O}_B, \tilde{x}_B, \tilde{y}_B, \tilde{z}_B)$;
return Geometry representation of the packed bed suitable for the snappyHexMesh utility

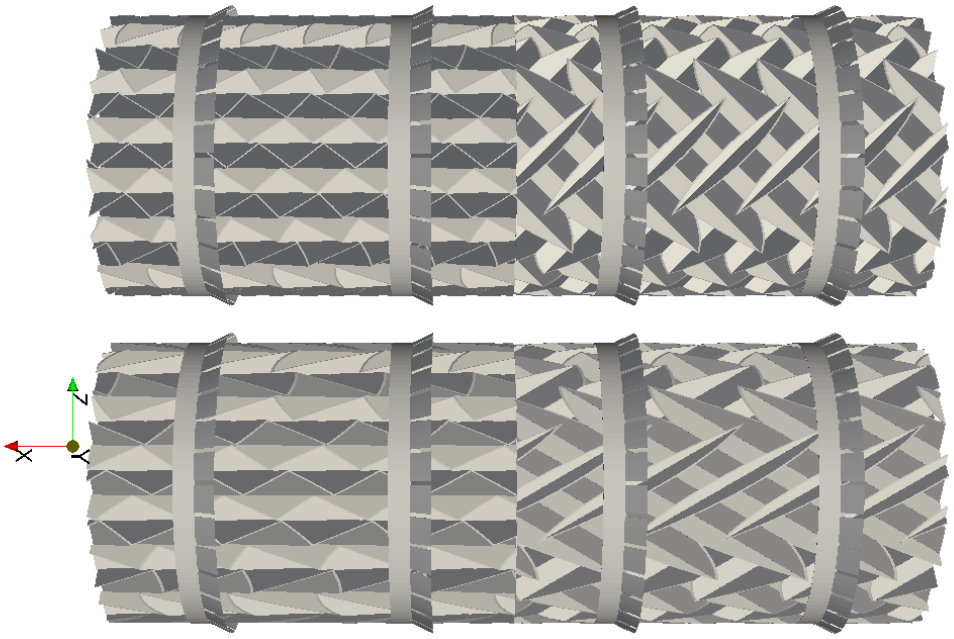

Figure 3: Geometry of a packed bed consisting of two unperforated Mellapak 250.Y/X (top/bottom) packing elements completed with four wall wipers.

even to industrial size problems.

Due to the need to adjust the mesh to the complex geometry, the resulting mesh is unstructured. More specifically, if we denote the cells of the base mesh as the cells with the refinement level $\mathcal{L}_0$, all the cells within 4 mm away from the geometry walls are refined to the level $\mathcal{L}_1$, where the refinement by one level corresponds to a splitting of the original cell to 8 approximately equivalent sub-cells. Moreover, all the cells within the distance 2 mm from the geometry walls are refined to the level $\mathcal{L}_2$. For the studied case of the packing diameter $D_{\mathrm{pk}} = 0.14\,\mathrm{m}$ and one packing element height $H_{\mathrm{pk}} = 0.2\,\mathrm{m}$ the resulting mesh size was of the order of millions cells per one packing element.

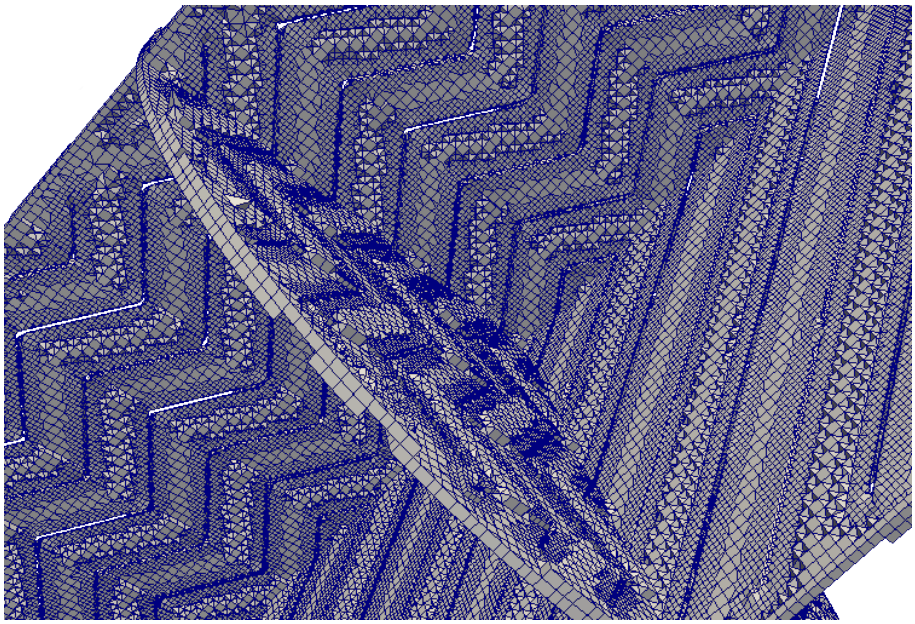

Figure 4: Mesh created for the Mellapak 250.Y packing. The depicted mesh has approximately $5.3 \cdot 10^6$ cells per one packing element. The cells with non-empty intersection with at least one of the planes $x = 0$, $y = 0$ and $z = 0$ are shown.

An example of the constructed mesh is depicted in Fig. 4. The mesh refinement in the vicinity of the geometry walls is well visible. Furthermore, it is possible to evaluate the mesh compliance with the packing geometry.

3 Model equations and simulation set-up

In all simulations, we considered a steady state in the case of a isothermal turbulent flow of an incompressible Newtonian fluid. All properties of the fluid were considered constant accross the whole computational domain. For the purposes of this investigation, we used the simpleFoam solver from the OpenFOAM toolbox. The simpleFoam is a steady state solver that uses the SIMPLE algorithm[8, 14] to compute the pressure-velocity coupling.

3.1 Governing equations

A stationary isothermic turbulent flow of an incompressible Newtonian fluid is described by the set of Navier-Stokes equations in the form,

$$\begin{aligned} \nabla \cdot (\mathbf{U} \otimes \mathbf{U}) - \nabla \cdot \mathbb{T} &= -\nabla p \\ \nabla \cdot \mathbf{U} &= 0\,, \end{aligned} \tag{1}$$

where $\mathbf{U}$ corresponds to the velocity field, p to the kinematic pressure and $\mathbb{T}$ to the viscous stress tensor defined as $\mathbb{T} = \nu \nabla \mathbf{U}$. The coefficient ν denotes the fluid kinematic viscosity. Please note, that we neglect all the body forces exerted on the fluid.

In order to take into account the effects of turbulence without having to resolve a transient problem with numerous length scales, we apply Reynolds averaging and rewrite the velocity and pressure as,

$$\begin{aligned} p &= \overline{p} + p' \\ \mathbf{U} &= \overline{\mathbf{U}} + \mathbf{U}' \,, \end{aligned} \tag{2}$$

where $\overline{p}$ and $\overline{\mathbf{U}}$ denote the averaged variables and p' and $\mathbf{U}'$ are the instantaneous fluctuations. The averaging itself may be done with respect to either time or space. Either way, the averaging operator has the following properties,

$$\begin{aligned} \overline{\left(\overline{\phi}\right)} &= \overline{\phi} \\ \overline{\phi'} &= 0 \\ \overline{\left(\overline{\phi}\overline{\psi}\right)} &= \overline{\phi}\,\overline{\psi} \\ \overline{\left(\overline{\phi}\psi'\right)} &= 0 \\ \overline{\left(\frac{\partial \phi'}{\partial s}\right)} &= 0 \,, \end{aligned} \tag{3}$$

where ϕ, ψ represent some flow functions. Furthermore, in the last relation of the equation (3), s may stand either for time or space coordinate.

Substituting for $\mathbf{U}$ and p in (1) from (2), while using the relations (3), one obtains the system,

$$\begin{aligned} \nabla \cdot \left(\overline{\mathbf{U}} \otimes \overline{\mathbf{U}}\right) - \nabla \cdot \left(\overline{\mathbb{T}} + \mathbb{T}'\right) &= -\nabla \overline{p} \\ \nabla \cdot \overline{\mathbf{U}} &= 0 \,, \end{aligned} \tag{4}$$

where the new variable, $\mathbb{T}'$, is the so called Reynolds stress tensor in the form $\mathbb{T}' = \mathbf{U}' \otimes \mathbf{U}'$.

Because of the presence of the non-linear Reynolds stress term, $\nabla \cdot \mathbb{T}'$, the formulation (4) requires additional modeling to be closed. In the present work, we select the Menter's $k-\omega$ shear stress transport (SST) model[13] in the formulation given by Hellsten[11] as the most suitable approach for the closure of the problem (4).

In the $k-\omega$ SST model, the closure problem is approached within the framework of the Boussinesq approximation[5, 22],

$$\mathbb{T}' = \nu_t \nabla \overline{\mathbf{U}} - \frac{2}{3}\mathbb{I}k \,, \tag{5}$$

where ν_t stands for the kinematic turbulent viscosity, $\mathbb{I}$ for the unit tensor and k for the kinetic energy of the turbulence. If one defines a modified kinematic pressure,

$$\tilde{p} = \overline{p} + \frac{2}{3}k \,, \tag{6}$$

it is possible to rewrite the equations (4) as

$$\begin{aligned} \nabla \cdot \left(\overline{\mathbf{U}} \otimes \overline{\mathbf{U}}\right) - \nabla \cdot \left(\nu_{\text{eff}} \nabla \cdot \overline{\mathbf{U}}\right) &= -\nabla \tilde{p} \\ \nabla \cdot \overline{\mathbf{U}} &= 0 \,, \end{aligned} \tag{7}$$

where $\nu_{\text{eff}} = \nu + \nu_t$ is the fluid effective kinematic viscosity. In the equations (7), there are two new variables, the turbulence kinetic energy, $k > 0$, and the kinematic turbulent viscosity, $\nu_t > 0$.

The $k-\omega$ SST model is a two-equation model; hence, two additional partial differential equations are solved together with the equations (7). The equations are added for the above introduced turbulence kinetic energy, k, and for the specific dissipation rate, $\omega > 0$, and read as follows,

$$\begin{aligned} \overline{\mathbf{U}} \cdot \nabla k &= P_k + \nabla \cdot \left[\left(\nu + \frac{\nu_t}{\sigma_k}\right)\nabla k\right] - \beta^* k\omega \\ \overline{\mathbf{U}} \cdot \nabla \omega &= P_\omega + \nabla \cdot \left[\left(\nu + \frac{\nu_t}{\sigma_{\omega,2}}\right)\nabla \omega\right] - F_2 \beta \omega^2 + 2\left(1 - F_1\right)\sigma_{\omega,2}\frac{1}{\omega}\nabla k \cdot \nabla \omega \end{aligned} \tag{8}$$

The model itself is a blend of the original $k-\omega$ model and of the $k-\epsilon$ model[22]. The blending is done through the function $F_1(k, \omega, y^+, \dots)$, which converges towards 1 ($k-\omega$ model) in the near-wall region (the dimensionless distance to the nearest wall y^+ is small) and towards 0 ($k-\epsilon$ model) in the free stream. Detailed specification of the model may be found for example in the work of Hellsten [11].

We will restrict the model description to the specification of the turbulent kinematic viscosity, ν_t, which appears in the equations (7). The turbulent kinematic viscosity of an incompressible fluid is in the $k-\omega$ SST model defined as,

$$\nu_t = \frac{a_1 k}{\max\left(a_1\omega; |\Omega_{ij}|F_3\right)}\,, \tag{9}$$

where a_1 is a model constant, F_3 is a limiter function, which improves the physicality of the solution[11] and $|\Omega_{ij}| = \sqrt{2\Omega_{ij}\Omega_{ij}}$ is the scalar measure of the vorticity tensor defined by

$$\Omega = \frac{1}{2}\left(\nabla\overline{\mathbf{U}} - \left(\nabla\overline{\mathbf{U}}\right)^{\mathrm{T}}\right)\,. \tag{10}$$

Finally, please note, that in the following we will omit the over-lines and tildes in the symbols notation.

3.2 Boundary conditions and initial guess

The system (7) – (8) needs to be completed with the suitable boundary conditions. The computational domain is defined as in section 2 and for the future reference will be denoted as $\mathcal{S}$. Also, we denote the boundary of $\mathcal{S}$ as $\partial\mathcal{S}$ and divide it into three different subdomains,

$$\partial\mathcal{S} \;=\; \partial\mathcal{S}_{\mathrm{inlet}} \cup \partial\mathcal{S}_{\mathrm{outlet}} \cup \partial\mathcal{S}_{\mathrm{wall}}\,. \tag{11}$$

Because the complete specification of the boundary conditions is given in Tab. 1, only a few explanatory notes will be given in the following text.

Boundary	Condition
$\mathcal{S}_{\mathrm{inlet}} = \{(x,y,z)\in\mathbb{R}^3 : x = h_{\mathrm{col}}, y^2+z^2 \le r_{\mathrm{col}}^2\}$	$\mathbf{U} = (-u_i, 0, 0)^{\mathrm{T}}, \quad \mathbf{S}_f\cdot\nabla p = 0$ $k = k_0, \quad \omega = \omega_0$
$\mathcal{S}_{\mathrm{outlet}} = \{(x,y,z)\in\mathbb{R}^3 : x = -h_{\mathrm{col}}, y^2+z^2 \le r_{\mathrm{col}}^2\}$	$\mathbf{S}_f\cdot\nabla\mathbf{U} = (0,0,0)^{\mathrm{T}}$ if $\mathbf{\Phi} > 0$, $\mathbf{U} = (0,0,0)^{\mathrm{T}}$ else $p = 0$ $\mathbf{S}_f\cdot\nabla k = 0$ if $\mathbf{\Phi} > 0$, $k = k_0$ else $\mathbf{S}_f\cdot\nabla\omega = 0$ if $\mathbf{\Phi} > 0$, $\omega = \omega_0$ else $\mathbf{\Phi} = \mathbf{S}_f\cdot\mathbf{U}$
$\mathcal{S}_{\mathrm{wall}} = B \cup \{(x,y,z)\in\mathbb{R}^3 : x = \langle -h_{\mathrm{col}}, -h_{\mathrm{col}}\rangle, y^2+z^2 = r_{\mathrm{col}}^2\}$	$\mathbf{U} = (0,0,0)^{\mathrm{T}}, \quad \mathbf{S}_f\cdot\nabla p = 0$ $\mathbf{S}_f\cdot\nabla k = 0, \quad \mathbf{S}_f\cdot\nabla\omega = 0$

Table 1: Applied boundary conditions. The column height and diameter are denoted as h_{col} and r_{col}, respectively. Symbol $\mathbf{S}_f$ denotes the outer normal vector to the boundary.

At the inlet, we prescribed Dirichlet boundary conditions for the velocity, $\mathbf{U}$, turbulent kinematic energy k, and the specific dissipation rate ω. Although it would be possible to prescribe more complex and physical inlet boundary conditions, based on the work of Khosravi-Nikou and Eshani [12] and our own tests, we concluded, that the error caused directly by the used boundary conditions is negligible.

At the outlet, we specified an inlet-outlet boundary conditions for $\mathbf{U}$, k and ω. The inlet-outlet boundary condition prescribes a zero-gradient Neumann type boundary condition for the case of the fluid outflow defined as $\mathbf{\Phi} = \mathbf{S}_f\cdot\mathbf{U} > 0$, where $\mathbf{S}_f$ is the outer normal to the boundary. Otherwise, a Dirichlet type boundary condition is prescribed. Furthermore, we fixed the pressure at the outlet by a Dirichlet type boundary condition.

On the walls, which consist of the column hull and the packing itself, we prescribed a standard no-slip boundary condition for the velocity and the zero-gradient boundary condition for the pressure. Furthermore, the mesh was refined in the way, that the nearest cells to the wall boundaries

lie within the flow laminar sublayer. Hence, we did not need to apply any special wall functions to the turbulence variables k and ω.

The problem specification was completed by the prescribed initial guess,

$$\mathbf{U}^{(0)} = (0,0,0)^{\mathrm{T}}, \quad p^{(0)} = 0, \quad k^{(0)} = k_0, \quad \omega^{(0)} = \omega_0, \quad \forall \boldsymbol{x} \in \mathcal{S}\,, \tag{12}$$

where the initial guesses for k and ω were estimated via the following relations,

$$\begin{aligned} k_0 &= \frac{3}{2}\left(u_f I_0\right)^2, & I_0 &= 0.0853\mathrm{Re}^{-0.0727}, \\ \mathrm{Re} &= \frac{u_f d_h}{\nu}, & u_f &= \frac{u_i}{\varepsilon_{\mathrm{pk}} \sin \alpha_{\mathrm{ch}}}, \\ \omega_0 &= \frac{\epsilon_0}{k_0}, & \epsilon_0 &= \frac{0.1643 k_0^{3/2}}{0.07 d_h}. \end{aligned} \tag{13}$$

In the above equations, u_f denotes an estimate of the mean free stream velocity in a packing channel calculated from the gas inlet velocity, u_i, the structured packing porosity, $\varepsilon_{\mathrm{pk}}$, and the channel inclination angle, α_{ch}. The symbol I_0 stands for the turbulence intensity and it is approximated using the formula of Russo and Basse [18] for the flow in a smooth pipe, which is based on the flow Reynolds number, Re. The used Reynolds number is evaluated from the estimate for the free stream velocity in the channels, u_f, the channels hydraulic diameter, h_d, and the fluid kinematic viscosity, ν.

4 Results and Discussion

In this section, we first present results of the mesh independence study performed to determine how fine a grid is required to capture the important flow physics. Then, we will proceed to the model validation, which is done through a comparison of measured and calculated dry pressure losses. The dry pressure loss is a difference between the pressures above and bellow the packed bed relative to the height of the packed bed,

$$\Delta p_h := \frac{p_{\mathrm{above}} - p_{\mathrm{bellow}}}{N_{\mathrm{pk}} H_{\mathrm{pk}}}\,. \tag{14}$$

After the model validation, we present results on the flow behavior in the Mellapak type packings, including the packing gas mixing capabilities.

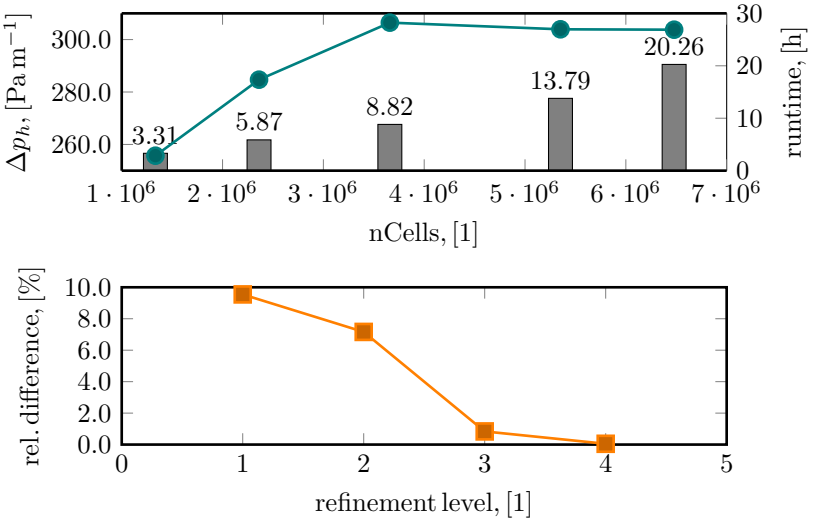

Figure 5: Mesh size independence study. The tests were performed for the N_2 gas, $u_i = 3.05\,\mathrm{m\,s^{-1}}$, and one element of the Mellapak 250.Y packing.

4.1 Mesh size independence

The calculated dry pressure loss for the selected mesh sizes as well as the simulations runtimes on 4 cores of the Altix UV2000 commercial cluster are depicted in the top part of Fig. 5. At the beginning, the calculated pressure loss increased with the mesh refinement. However, with the number of cells in the mesh around $4 \cdot 10^6$, the dry pressure loss stabilized. More specifically, the difference between the Δp_h calculated on the mesh with approximately $5.3 \cdot 10^6$ cells per one packing element and the Δp_h calculated on the mesh with approximately $6.4 \cdot 10^6$ cells per packing element was less then 0.5%. Hence, for the calculations, we used the meshes with the size corresponding to $5.3 \cdot 10^6$ cells per one packing element.

4.2 Model validation

The model validation was done on experimental data measured in a semi-industrial absorption column with the diameter $D_{\mathrm{col}} = 0.15\,\mathrm{m}$. The packed bed consisted of 6 packing elements of either Mellapak 250.X or Mellapak 250.Y and had the total height of $H_{\mathrm{pk}} = 1.26\,\mathrm{m}$. The used packing had the diameter $D_{\mathrm{pk}} = 0.14\,\mathrm{m}$. The experiments were performed for three different gases, He, N_2 and SF_6, which differ mostly by their density and consequently also by their kinematic viscosity. The properties of the used gases are summarized in Tab. 2

Gas	μ, $10^{-5}\,[\mathrm{Pa\,s}]$	ρ, $[\mathrm{kg\,m^{-3}}]$	ν, $10^{-5}\,[\mathrm{m^2 s^{-1}}]$	u_i range, $[\mathrm{m\,s^{-1}}]$	Packing type
N_2	1.75	1.149	1.52	$\langle 0.46, 4.34 \rangle$	X,Y
He_2	2.00	0.190	10.5	$\langle 1.05, 6.81 \rangle$	X,Y
SF_6	1.55	5.648	0.274	$\langle 0.28, 1.94 \rangle$	Y

Table 2: Properties of the gases used for the model validation.

The gas inlet velocities ranged from approximately $0.4\,\mathrm{m\,s^{-1}}$ to approximately $6.8\,\mathrm{m\,s^{-1}}$. The lower bound of the gas velocity was determined by the sensitivity of the used barometer, the upper bound was due to the used fan power.

The model geometry was designed to match the experimental set up as much as possible. The only difference was the lack the lack of wall wipers in the model geometry. Furthermore, also the fluid properties were fixed as close as possible to the real gases. In Fig. 6, we compare the measured and calculated Δp_h for all the available data.

For the Mellapak 250.Y cases, the relative difference between the measured and estimated values,

$$\mathcal{E}_R := \frac{\left| \Delta p_h^{\mathrm{Exp.}} - \Delta p_h^{\mathrm{CFD}} \right|}{\Delta p_h^{\mathrm{Exp.}}} \cdot 100\%\,, \tag{15}$$

was usually bellow 10%. The only exceptions were the measurements with extremely low gas flow rates, where the $\mathcal{E}_R$ might go up to 30%. On the other hand, as the $\Delta p_h^{\mathrm{Exp.}}$ was close to the lowest measurable value, the experimental data in these cases could be burdened with some error.

For the Mellapak 250.X cases, the model tends to underestimate Δp_h, in the worst scenario encountered for the N_2 gas by approximately 30%. We assumed, that such a behavior might have two main causes.

As a first cause, we identified the lack of wall wipers in the model geometry. In reality, the Mellapak packing wall wipers are made out of a dense steel net. Hence, the permeability of the wall wipers material for the gas flow depends on the angle of attack. For the case of the angle of attack close to $\pi/2$, the material is well permeable. On the other hand, for the angle of attack approaching either 0 or π, the material is almost completely impermeable. As a consequence, the effects of wall wipers on Δp_h is stronger for Mellapak 250.X packing, in which the angle of attack on the wall wiper is close to $\pi/6$, compared to Mellapak 250.Y packing, with the angle of attack approximately $\pi/4$.

We thought that the second reason was the number of the used packing elements. For the data depicted in Fig. 6, we simulated only one packing element. For the combination of the used overall packing dimensions ($H_{\mathrm{pk}} = 0.21\,\mathrm{m}$, $D_{\mathrm{pk}} = 0.14\,\mathrm{m}$, $D_{\mathrm{col}} = 0.15\,\mathrm{m}$), this means, that there

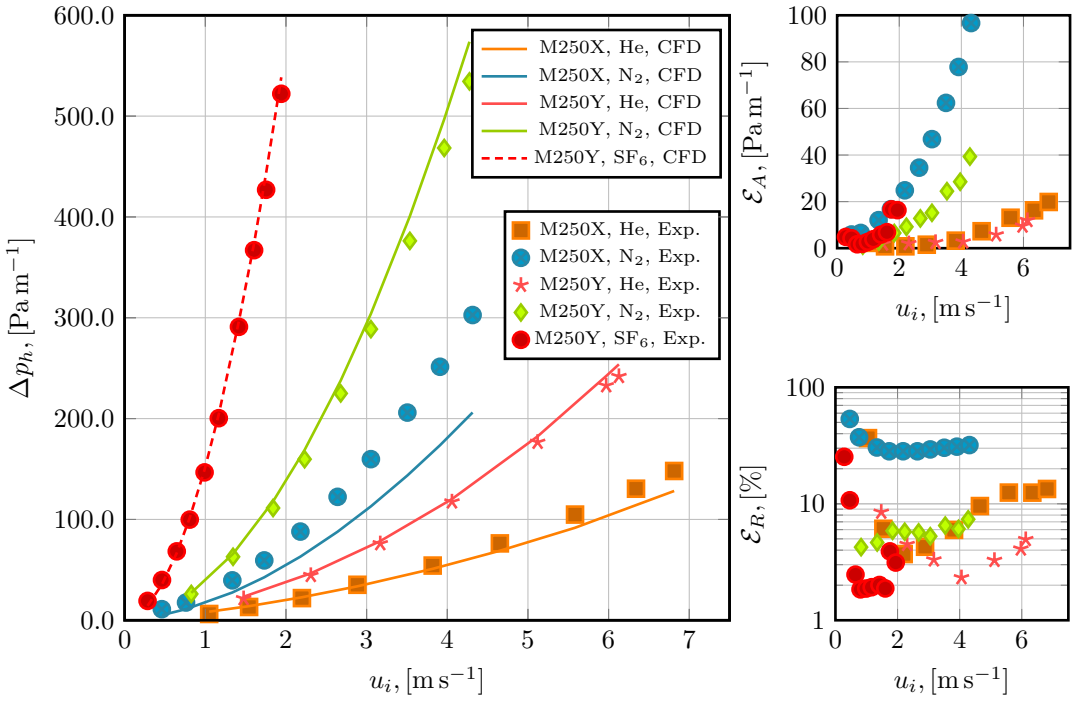

Figure 6: Results of the model validation obtained on one packing element. In the left part of the figure, there are directly compared measured and calculated dry pressure losses. In the top right subplot, we depict the absolute differences between the experiment and CFD. In the bottom right subplot, the corresponding relative differences are shown.

exists a few channels that go through the whole geometry without encountering any of the column outer hull. Thus, the gas flowing through these channels is not forced to change the flow direction within the simulated domain. As the forced changes in the gas flow direction are, together with the friction on the walls, the main cause for the flow energy dissipation, the presence of such channels was assumed to cause the underestimation of the packing dry pressure loss.

Nevertheless, the comparison of the dry pressure loss calculated on one and two packing elements, shown in Fig. 7, disproved our hypothesis. In most cases, the relative difference between the calculated pressure losses is around or less than 1%. Thus, it cannot explain the difference between the measured and estimated Δp_h for the N_2 gas flow through the Mellapak 250.X, which is around 30%. On the other hand, we confirmed that for the Δp_h estimation, it is sufficient to simulate a single packing element.

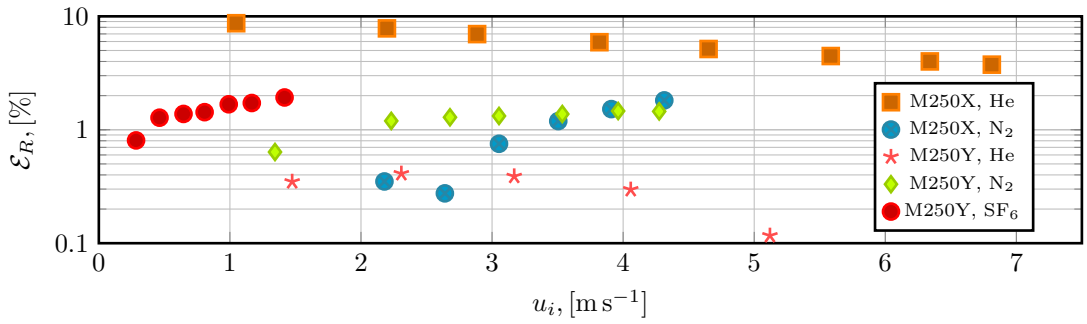

Figure 7: Comparison of the relative difference between the calculated Δp_h for one and two packing elements.

4.3 Gas mixing properties of studied packings

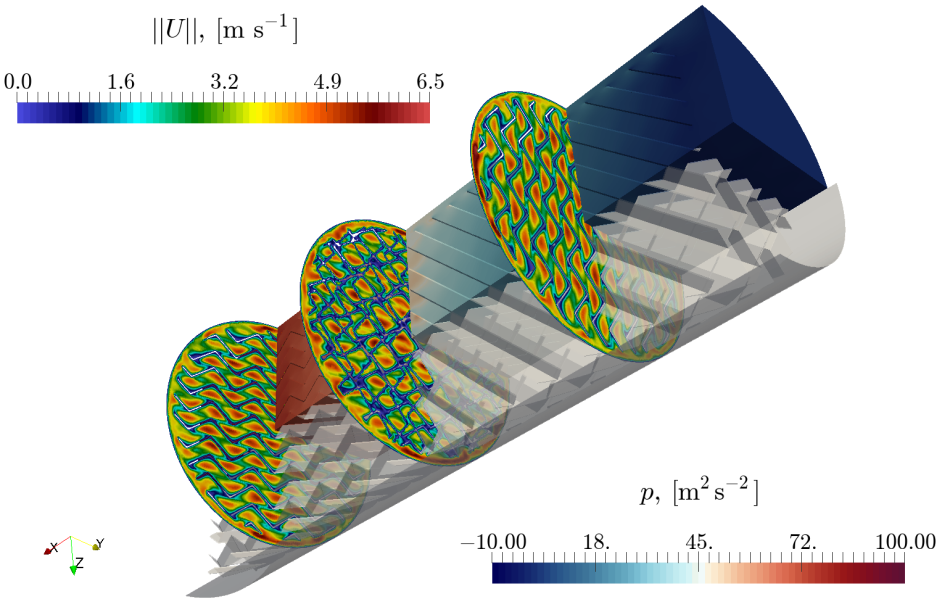

Figure 8: Pressure and velocity field in the Mellapak 250.Y packing. The depicted results were calculated on two packing elements for He, $u_i = 2.30\,\mathrm{m\,s^{-1}}$, Re = 280.

Via the validated model, we studied the flow characteristics of the gas in Mellapak 250.X and Mellapak 250.Y packings. An example of the obtained qualitative results is depicted in Fig. 8. The clip in the back of Fig. 8 shows an example of the kinematic pressure distribution in the computational domain. Here, we would like to emphasize the visibly higher pressure at the entrance to the channels, as well as a relatively low pressure drop caused directly by the transfer from one packing element to another. The latter result corresponds well with the above noted good agreement between the pressure losses calculated on one and two packing elements.

The slices through the geometry made at $x = \{-0.13, 0.00, 0.13\}\,\mathrm{m}$ show the main flow patterns inside the structured packing. One may notice a rotation of the principal plane of the flow between the first slice at $x = +0.13\,\mathrm{m}$ and the last one at $x = -0.13\,\mathrm{m}$ by 90°, which corresponds to the angle between the two packing elements, φ_{pk}. The middle slice is placed directly at the contact of the two elements and shows the transition region between the two regular flows.

Within the limitations of the performed Reynolds averaging, it is possible to conclude, that the flow in the studied structured packing is mostly irrotational (with the exceptions of the transition between the packing elements and the region close to the column outer hull) and highly regular. Interestingly, the gas remains in the original channel even during the contacts with the channels with different orientation (the channels appertaining to the neighbor packing sheet). In other words, there is no gas mixing at the channel-channel contact planes. More specifically, the contact plane between two channels with the opposite orientation, although it is in fact just a hypothetical boundary, it behaves as a wall moving parallel to the axis x.

Another possibility to evaluate the flow properties inside the structured packing is via the velocity streamlines. Without the loss of generality we define a streamline passing through the point $\boldsymbol{x}_0$ as

$$\gamma_{\boldsymbol{x}_0} = \left\{ \boldsymbol{x} \in \mathcal{S} : \frac{\mathrm{d}\,\boldsymbol{x}}{\mathrm{d}\,t} \times \mathbf{U} = 0, \boldsymbol{x}(t=0) = \boldsymbol{x}_0 \right\} \tag{16}$$

and the set of all the streamlines passing through a seed domain, σ, as

$$\Gamma_\sigma = \{ \gamma_{\boldsymbol{x}} \in \mathcal{S} : \boldsymbol{x} \in \sigma \}\,. \tag{17}$$

In Fig. 9, we compare the streamlines obtained in the Mellapak 250.Y geometry for two different

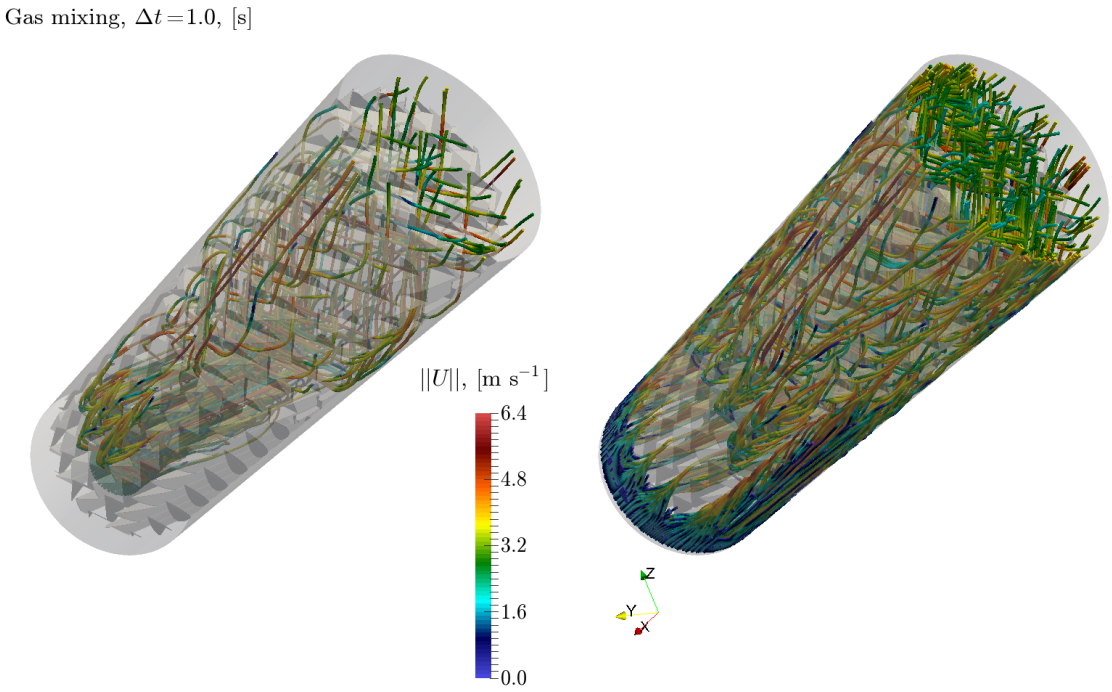

Figure 9: Mixing of the gas in the Mellapak 250.Y packing. The depicted results were calculated on two packing elements for He, $u_i = 2.30\,\mathrm{m\,s^{-1}}$, Re = 280.

seed domains,

$$\begin{aligned} \sigma_1 &= \{(x,y,z) \in \mathcal{S} : x = -0.22\,\mathrm{m}, y^2 + z^2 \leq 0.025^2\,\mathrm{m}\} \\ \sigma_2 &= \{(x,y,z) \in \mathcal{S} : x = -0.22\,\mathrm{m}, 0.07^2\mathrm{m} \leq y^2 + z^2 \leq 0.075^2\,\mathrm{m}\}\,. \end{aligned} \tag{18}$$

The first seed domain, σ_1, represents a circle with the diameter $D_{\sigma_1} = 0.05\,\mathrm{m}$ placed one centimeter bellow the packed bed. The seed domain σ_2 corresponds to an annulus placed one centimeter bellow the packed bed. The dimensions of the annulus were chosen in the way, that it fits into the gap between the packing and the column outer hull. Because of the seeds selection, it is possible to qualitatively study the mixing properties of the Mellapak 250.Y packing.

To study the mixing properties of the structured packing, we propose to introduce a notion of the distribution of the streamlines passing through a seed source σ in a control volume, $\omega \in \mathcal{S}$. Let us denote the discrete representation of the computational domain $\mathcal{S}$ as $\mathcal{S}^h$. The discrete computational domain (i.e. the mesh) consists of M non-overlapping cells, $\boldsymbol{x}_i^h$, of volumes $\mathcal{V}(\boldsymbol{x}_i^h)$. Hence, in the discrete setting it is possible to introduce a volume of the discrete representation of the trajectory $\gamma_{\boldsymbol{x}}$ as follows,

$$\mathcal{V}(\gamma_{\boldsymbol{x}}^h) = \sum_{\boldsymbol{x}_i^h \in \gamma_{\boldsymbol{x}}^h} \mathcal{V}(\boldsymbol{x}_i^h), \tag{19}$$

where $\gamma_{\boldsymbol{x}}^h$ is the above mentioned discrete representation of the trajectory $\gamma_{\boldsymbol{x}}$. Furthermore, the volume of the discrete domain ω^h is

$$\mathcal{V}(\omega^h) = \sum_{\boldsymbol{x}_i^h \in \omega^h} \mathcal{V}(\boldsymbol{x}_i^h)\,. \tag{20}$$

Finally, it is possible to calculate the fraction of $\mathcal{V}(\omega^h)$ occupied by the trajectories Γ_σ^h,

$$\varrho_\sigma^\omega = \frac{\mathcal{V}(\Gamma_\sigma^h \cap \omega^h)}{\mathcal{V}(\omega^h)}\,. \tag{21}$$

Definition 1 *We say, that the trajectories are uniformly distributed in some domain $\mathcal{S}^h$, if $\varrho_\sigma^\omega = \varrho_\sigma^S \,\forall\, \omega^h \subseteq \mathcal{S}^h$.*

Remark 1 *Please note, that the above definition is relevant strictly to the discrete setting and does not hold asymptotically. For example, the selection of ω^h is not completely unconstrained, as it is limited by the size of the discretization cells.*

After passing through two packing elements, the streamlines are rather uniformly distributed for both the selected seeds, as it might be seen in Fig. 9. However, the uniform streamlines distribution seems to be obtained more quickly for the gas entering to the column near the outer hull.

For the case of σ_1, depicted in the left side of Fig. 9, the gas enters directly only a few channels in the center of the packed bed. However, at the exit from these channels, the gas does not re-enter only the channels directly above, but rather a several channels close to the original channels exit. As a result, the ratio of the number of the exited channels to the number of the newly entered channels is lower than one. The fact that at each encounter with the column outer hull the gas enters more channels, than it exits causes, that at the outlet from the first packing element the streamlines are uniformly distributed along the y axis. However, as the channels in the first packing element are oriented parallel to the $z = 0$ plane, the gas is not transported along the z axis. On the other hand, at the entrance to the second packing element, the gas, already evenly distributed along the y axis, enters all the available channels that are oriented parallel to the $y = 0$ plane. As a result, the streamlines distribution at the outlet from the second packing element is approximately uniform.

Regarding the case of σ_2, the gas starts by sliding along the column outer hull and enters the first packing element not directly from the bottom, but rather from sides. Consequently, the equalization of the streamlines distribution along the y axis is quicker. Furthermore, the gas enters the channels of the first packing element all across the z axis. Hence, the trajectories are more or less uniformly distributed already at the outlet from the first packing element.

5 Conclusions

Even nowadays, the distillation remains the most energy-intensive technology of the chemical industry. Nevertheless, the design of the distillation columns remains mostly empirical. In an attempt to shed some light on the intricacies of the gas flow in the widely used commercial packings, Mellapak 250.X and Mellapak 250.Y, we provided a relatively quick and accurate method to generate a geometric representation of these packings. Furthermore, we constructed a CFD model for the gas flow through the structured packing. We validated the model on the available experimental data and used it to study the flow characteristics in the Mellapak type structured packings. In the future research, we would like to concentrate on the modeling of the multiphase flow in the Mellapak type packings as well as on the development of the models for the flow in random packings.

Acknowledgments: The work of M. Isoz was supported by the Centre of Excellence for nonlinear dynamic behaviour of advanced materials in engineering CZ.02.1.01/0.0/0.0/15_003/0000493 (Excellent Research Teams) in the framework of Operational Programme Research, Development and Education. Moreover, the author thankfully acknowledges financial support from IGA of UCT Prague, grant numbers A2_FTOP_2016_024 and A1_FCHI_2016_004 and from the Czech Science Foundation, grant number GACR 13-01251S. Finally, the author would like to express his deepest thanks to the Mass Transfer Laboratory of UCT Prague for providing theirs, yet unpublished, experimental data for the model validation.

References

[1] Y. Amini, J. Karimi-Sabet, and M. N. Esfahany. Experimental and numerical simulation of dry pressure drop in high-capacity structured packings. *Chem. Eng. Technol.*, 39:1161–1170, 2016.

[2] H. Bai, J. Theuerkauf, and P. A. Gillis. A coupled DEM and CFD simulation flow field and pressure drop in fixed bed reactor with randomly packed catalyst particles. *Ind. Eng. Chem. Res.*, 48:4060–4074, 2009.

[3] M. J. Baker. *CFD simulation of flow through packed beds using the finite volume technique.* dissertation, University of Exeter, 2011.

[4] P. Bertoldi, J. L. Lorente, and N. Labanca. Energy consumtion and energy efficiency trends in the EU-28 2000-2014. Technical Report EUR 27972 EN, EU, 2016.

[5] R. B. Bird, W. E. Stewart, and E. N. Lightfoot. *Transport Phenomena.* Wiley & Sons, Madison, Wisconsin, 2 edition, 2002. ISBN 0-471-41077-2.

[6] J. J. Cooke, S. Gu, L. M. Armstrong, and K. H. Luo. Gas-liquid flow on smooth and textured inclined planes. *World. Ac. of Sc., Eng. and Technol.*, 68:1712–1719, 2012.

[7] Y. Demirel. Sustainable operations for distillation columns. *Chem. Eng. Process Tech.*, 1:15, 2013.

[8] J. H. Ferziger and M. Peric. *Computational methods for fluid dynamics.* Springer-Verlag, Berlin, Germany, 3 edition, 2002. ISBN 3-540-42074-6.

[9] Y. Haroun and L. Raynal. Use of computational fluid dynamics for absorption packed column design. *Oil Gas Sc. Technol.*, 71:18, 2016.

[10] Y. Haroun, L. Raynal, and P. Alix. Prediction of effective area and liquid hold-up in structured packings by CFD. *Chem. Eng. Res. and Des.*, 92:2247–2254, 2014.

[11] A. Hellsten. Some improvements in Menter's k-ω SST turbulence model. In *Proceedings of the Fluid Dynamics Conference*, volume 71, page 11. AIAA, 1997.

[12] M. R. Khosravi-Nikou and M. R. Eshani. Turbulence models application on CFD simulation of hydrodynamics, heat and mass transfer in a structured packing. *Int. Comm. Heat Mass Tr.*, 17:21, 2008.

[13] F. R. Menter. Improved two.equation k-ω turbulence models for aerodynamic flows. Technical Report N93-22809, NASA, 1992.

[14] F. Moukalled, M. Darwish, and L. Mangani. *The finite volume method in computational fluid dynamics: an advanced introduction with OpenFOAM and Matlab.* Springer-Verlag, Berlin, Germany, 1 edition, 2016. ISBN 978-3-319-16874-6.

[15] S. A. Owens, M. R. Perkins, R. B. Eldridge, K. W. Schulz, and R. A. Ketcham. Computational fluid dynamics simulation of structured packing. *Ind. Eng. Chem. Res.*, 52:2032–2045, 2013.

[16] M. M. Parizi and R. Rahimi. Hydrodynamics of sieve tray distillation column using CFD simulation. *J. Chem. Petr. Eng.*, 49:119–129, 2015.

[17] L. Raynal and A. Royon-Lebeaud. A multi-scale approach for cfd calculations of gas-liquid flow within large size column equipped with structured packing. *Chem. Eng. Sci.*, 62(24): 7196–7204, 2007.

[18] F. Russo and N. T. Basse. Scaling of turbulence intensity for low-speed flow in smooth pipes. *Flow Meas. Inst.*, 52:101–114, 2016.

[19] J. D. Seader and E. J. Henley. *Separation process principles.* Wiley India Pvt. Limited, 2 edition, 2006. ISBN 9788126509270.

[20] D. Sebastia-Saez, S. Gu, and P. Ranganathan. 3D modeling of hydrodynamics and physical mass transfer characteristics of liquid flom flows in structured packing elements. *Int. J. of Greenhouse Gas Cont.*, 19:492–502, 2013.

[21] SET-Plan Secreatariat. Continue efforts to make EU industry less energy intensive and more competitive. Technical Report SET-Plan ACTION n° 6, EU, JRC – Institute for Energy and Transport, 2016.

[22] D. C. Wilcox. *Turbulence Modeling for CFD.* DCW Industries, La Canada, California, 1 edition, 1994. ISBN 0-9636051-0-0.